Intersensor Remote Sensing Image Registration Using Multispectral Semantic Embeddings

Ruben Fernandez-Beltran, Filiberto Pla, and Antonio Plaza, *Fellow, IEEE*

***Abstract*— This letter presents a novel intersensor registration framework specially designed to register Sentinel-3 (S3) operational data using the Sentinel-2 (S2) instrument as a reference. The substantially higher resolution of the Multispectral Instrument (MSI), on-board S2, with respect to the Ocean and Land Color Instrument (OLCI), carried by S3, makes the former sensor a suitable spatial reference to finely adjust OLCI products. Nonetheless, the important spectral–spatial differences between both instruments may constrain traditional registration mechanisms to effectively align data of such different nature. In this context, the proposed registration scheme advocates the use of a topic model-based embedding approach to conduct the intersensor registration task within a common multispectral semantic space, where the input imagery is represented according to their corresponding spectral feature patterns instead of the low-level attributes. Thus, the OLCI products can be effectively registered to the MSI reference data by aligning those hidden patterns that fundamentally express the same visual concepts across the sensors. The experiments, conducted over four different S2 and S3 operational data collections, reveal that the proposed approach provides performance advantages over six different intersensor registration counterparts.**

***Index Terms*— Image registration, multispectral imaging, remote sensing, Sentinel-2, Sentinel-3, topic modeling.**

I. Introduction

FROM early years, image registration has played a fundamental role in many remote sensing applications, where analyzing multiple images of the same scene is important. For instance, image fusion [1], change detection [2], scene classification [3], and image superresolution [4] are among the most popular applications where the lack of geometrical misalignments is a key factor. In general, the image registration process consists of overlaying two or more images of the same scene which have been acquired at different times, from different viewpoints or/and using different imaging sensors. More specifically, this process can be defined as geometrically transforming one or more input images, which are called slave images, to the coordinate system of a given reference image, known as a master image. In order to achieve this goal, four main steps are typically conducted by automatic registration algorithms [5]: 1) characterization; 2) matching; 3) transformation; and 4) projection. In the first step 1), the slave and master images are characterized by extracting distinctive image structures or features. In 2), the considered image characteristics are compared to one another in order to find the spatial correspondences according to a specific similarity criterion. In the third step 3), the transformation model is defined and the corresponding alignment parameters are estimated. Finally, the fourth step 4) deals with the generation of the modified version of the slave image by applying the previously estimated transformation and a particular interpolation function.

In the literature, it is possible to find two main trends when uncovering such transformations from airborne and space optical data [6]: area-based and feature-based methods. On the one hand, area-based registration techniques directly use pixel intensity values to find the geometric correspondence between the slave and master images by optimizing a specific similarity metric. Cross correlation (CC) and mutual information (MI) are the most popular metrics for registering monomodal and multimodal optical data, respectively. On the other hand, CC-like methods pursue to maximize the correlation over the image overlap, MI-based approaches aim at maximizing the degree of statistical dependence between the images, which eventually makes this kind of techniques more suitable for intersensor scenarios where intensity changes across sensors are logically expected [5]. Despite the inherent simplicity of the area-based registration approach, these methods are still in use because of their simple hardware implementation in real remote sensing environments [7], [8]. Nonetheless, the high computational demand when handling complex image distortions and data may constrain the straightforward nature of these characterization schemes. On the other hand, feature-based registration techniques make use of a set of representative points extracted from both slave and master images to reduce the amount of input data. These methods require defining how the corresponding interest points are located, characterized and paired according to a specific matching strategy. For instance, Ma *et al.* [9] presented a remote sensing image registration approach which employs a modified version of the scale-invariant feature transform (SIFT) algorithm, together with a robust key-point matching protocol that combines position, scale, and orientation to increase the number of significant correspondences. Another relevant work can be found in [10], where Fan *et al.* define a novel matching algorithm specifically designed for synthetic aperture radar (SAR) imagery. In particular, this approach makes

Manuscript received December 26, 2018; revised February 13, 2019; accepted March 11, 2019. Date of publication April 2, 2019; date of current version September 25, 2019. This work was supported by Generalitat Valenciana (APOSTD/2017/007), the Spanish Ministry of Economy (ESP2016-79503-C2-2-P, TIN2015-63646-C5-5-R), Junta de Extremadura (Ref. GR18060) and the European Union under the H2020 EOXPOSURE project (No. 734541). *(Corresponding author: Ruben Fernandez-Beltran.)*

R. Fernandez-Beltran and F. Pla are with the Institute of New Imaging Technologies, University Jaume I, 12071 Castellón de la Plana, Spain (e-mail: rufernan@uji.es; pla@uji.es).

A. Plaza is with the Hyperspectral Computing Laboratory, Department of Technology of Computers and Communications, Escuela Politécnica, University of Extremadura, 10003 Cáceres, Spain (e-mail: aplaza@unex.es).

Color versions of one or more of the figures in this letter are available online at http://ieeexplore.ieee.org.

Digital Object Identifier 10.1109/LGRS.2019.2904874

use of a patch-based descriptor that includes local intensity values as well as geometric features to relieve the speckle noise effect when coregistering SAR data. Yang *et al.* [11] use a multiscale deep-learning architecture to uncover more representative feature points to register multitemporal remote sensing data.

Despite the potential of all these approaches, the inherent complexity of the multispectral image domain, together with the peculiarities of the real-world sensed data, still raise some challenges when registering airborne and space optical data from different operational instruments. Note that the registration of large Earth surface areas becomes particularly challenging when considering rather different spectral–spatial image resolutions, and hence, certain data relaxations may be useful in operational scenarios [6]. Yan *et al.* [12] introduce two main data simplifications when registering Landsat-8 OLI and Sentinel-2 MSI operational data in order to reduce the process complexity while also obtaining a subpixel precision. First, the authors only consider the near-infrared (NIR) bands to estimate the intersensor displacements. Second, these displacements are effectively modeled by affine transformations.

Another important reason to simplify the problem intricacy in operational environments is the increasing demand for on-board imaging applications. Some of the most widely used processing techniques, including the image registration task, are recommended to be conducted from an on-board perspective in order to relieve the ground-segment workload. Nonetheless, the physical limitations of the hardware carried by remote sensing platforms may impose important operational constraints that motivate the use of simplified versions of the data registration process. Specifically, a common practice consists in conducting band-to-band registration in order to align each slave image band to the closest master one. Zhang *et al.* [13] propose to register ZiYuan-3 and GeoEye-1 multispectral operational data considering the corresponding panchromatic images as reference. However, this band-to-band strategy requires a suitable spectral connection between sensing instruments, which may not be always possible. Alternative methods show the effectiveness of reducing the input data dimensionality by means of shared intersensor projection spaces. This is the case of the work presented by Goncalves *et al.* [14] which makes use of the principal component analysis (PCA) transformation to project and register remote sensing data. Notwithstanding the remarkable performance achieved by these methods in actual operational scenarios, there is still room for improvement because of the high complexity of unifying rather different spectral information into a common characterization space when conducting intersensor registration. This is particularly the case for the most important currently operational Earth Observation missions where Copernicus plays an important role.

The Copernicus programme is a joint action of the European Commission, the European Space Agency and the European Environment Agency in order to supply continuous Earth information for environmental and security applications. Within the program resources, Sentinel-2 (S2) [7] and Sentinel-3 (S3) [8] missions are focused on the global monitoring of the Earth surface by means of multispectral imagery, and hence, both operations share important synergies. The S2 mission includes two identical satellites (S2A and S2B) which incorporate the Multispectral Instrument (MSI) imaging sensor. This instrument provides 13 bands spanning from 443- to 2190-nm spectral range, with spatial resolution up to 10 m per pixel (mpp). Analogously, the S3 mission comprises a pair of dedicated satellites (S3A and S3B) that carry the Ocean and Land Color Instrument (OLCI) sensor that provides 21 spectral bands ranging from 400 to 1020 nm, with spatial pixel size of 300 mpp. Being the spatial resolution of the MSI substantially higher than the OLCI's creates an ideal scenario to conduct an intersensor image registration process where the higher spatial resolution of the former sensor can be used to correct possible global misalignments in the latter.

In that scenario, this letter proposes a novel intersensor image registration framework that makes use of a semantic embedding space based on probabilistic topic models to improve the functional registration scheme when considering S2 MSI and S3 OLCI operational data. From an intersensor perspective, registration mechanisms require a particular spectral association to conduct the registration process. However, this connection may be difficult to define in actual production environments, or even it may become ineffective when involving sensors of a rather different nature, such could be the case of MSI and OLCI. Topic models have been successfully used in remote sensing due to their potential to effectively manage airborne and space optical data at a higher abstraction level, being probabilistic latent semantic analysis (pLSA) one of the most effective models [15]. Nonetheless, this kind of probabilistic models has not yet been used to register intersensor data despite their capability to relate visual semantic information [16], which may be a key factor to overcome intersensor dissimilarities. From a practical perspective, topic models aim at uncovering hidden generative patterns (known as topics) from an input data set, and also to express the whole data collection as a probability distribution of topics instead of the observable low-level features. The main issue when registering intersensor imagery is the fact that the slave and master multispectral domains are not the same since they are both defined by different imaging sensors. To address this issue, we develop a novel intersensor registration scheme that projects the multisource input data into a topic-based semantic embedding, where the registration process can be conducted according to the uncovered spectral patterns. Our experiments, which include operational S2 MSI and S3 OLCI data and six different registration alternatives, show the advantages of the proposed approach for intersensor image registration.

II. Methodology

A. Intersensor Image Registration Framework

The proposed S2 and S3 intersensor image registration frameworks consist of the following three steps (Fig. 1).

1) *Data Preparation:* Two different encoding procedures are adopted to unify S2 MSI and S3 OLCI spatial resolutions. On the one hand, a straightforward pixel-wise characterization approach is used for S3, where spatial pixels represent topic model documents (d) and unsigned integer 16-bit band reflectance values serve as the model word-counts ($n(w, d)$). On the other hand, a bag-of-words approach [1] is conducted to encapsulate S2 voxels, representing S3 pixels, as histograms

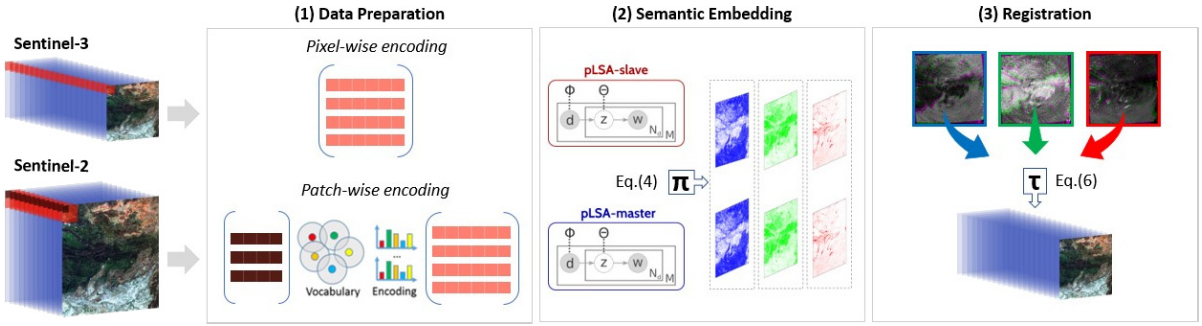

Fig. 1. Proposed Sentinel-2 and Sentinel-3 intersensor image registration framework.

of visual words. Note that the scaling ratio between both instruments is set beforehand due to the prior knowledge of the relative sensor resolutions, which is 15× in this letter. Initially, S2 data are characterized as vectorized $3 \times 3 \times 13$ image patches with one pixel overlapping. Then, the k-means clustering algorithm is globally applied to these primitive features in order to define the visual vocabulary containing 100 clusters. This setting provides a fine granularity of S2 spectral patterns [1]. Subsequently, the S2 image is tiled into $15 \times 15 \times 13$ image patches. Finally, the S2 local primitive features ($3 \times 3 \times 13$) within each S3 pixel ($15 \times 15 \times 13$) are encoded as a single histogram of visual words by accumulating the number of local features into their closest cluster. From this process, we obtain two different collections of M documents: one for S3, $\mathbf{D}_3 \in \mathbb{N}^{M \times 21}$, and another for S2, $\mathbf{D}_2 \in \mathbb{N}^{M \times 100}$. Note that M represents the number of spatial pixels in S3 and also the number of 15×15 voxels in S2.

2) *Semantic Embedding:* Following the asymmetric formulation of the standard pLSA model [17], we estimate the $\mathbf{\Phi} \sim p(z|d)$ and $\mathbf{\Theta} \sim p(w|z)$ parameters for both $\mathbf{D}_3$ and $\mathbf{D}_2$ collections by maximizing the complete log-likelihood function using the expectation–maximization (EM) algorithm. In particular, the EM procedure works in two iterative stages: the E-step (1), where the expected likelihood value is calculated given the current parameter estimates, and the M-step (2)–(3), where the new optimal parameter values are computed according to the current state. In this letter, we use a hidden latent space with 3 units ($Z = 3$) and 1000 EM iterations as default convergence settings

$$p(z|w,d) = \frac{p(z,w,d)}{p(w,d)} = \frac{p(w|z)p(z|d)}{\sum_z p(w|z)p(z|d)} \quad (1)$$

$$\mathbf{\Phi} \sim p(z|d) = \frac{\sum_w n(w,d)p(z|w,d)}{\sum_z \sum_w n(w,d)p(z|w,d)} \quad (2)$$

$$\mathbf{\Theta} \sim p(w|z) = \frac{\sum_d n(w,d)p(z|w,d)}{\sum_w \sum_d n(w,d)p(z|w,d)}. \quad (3)$$

Since $\mathbf{D}_2$ and $\mathbf{D}_3$ collections are independently processed to estimate $\mathbf{\Phi}_2 \in \mathbb{R}^{M \times Z}$ and $\mathbf{\Phi}_3 \in \mathbb{R}^{M \times Z}$, respectively, we conduct an additional postprocessing optimization step to align both semantic characterizations, that is, sorting the slave topic-document representation according to the master one. We find the optimal permutation matrix $\mathbf{\Pi}$ that minimizes the intersensor topic-document ℓ_2 norm as (4) shows. Finally, (5) is used to apply such permutation to $\mathbf{\Phi}_3$. Note that the numeric subscripts are used to identify S2 and S3 parameters

$$\mathbf{\Pi} = \arg\min_{\mathbf{\Pi}^*} \| \Phi_2 - \mathbf{\Pi}^* \Phi_3 \|_2 \quad (4)$$

$$\Phi_3 = (\mathbf{\Pi}\, \Phi_3). \quad (5)$$

3) *Registration:* This step estimates the misalignment between the master and slave images and also estimates the final registered result. In particular, a straightforward band-to-band registration approach [12] has been adopted, considering an affine transformation model together with the MI metric and the One Plus One Evolutionary Optimizer [18] in order to estimate the corresponding displacements between the paired topic characterizations. Then, the global transformation $\overline{\tau}$ between the master and slave images is computed as

$$\overline{\tau} = \sum_i \frac{\tau\left(\Phi_2^i, \Phi_3^i\right)}{Z} \quad (6)$$

where the τ operator estimates the affine displacement according to the aforementioned MI-based registration process, Φ_2^i and Φ_3^i represent the ith document-topic characterizations for S2 and S3 and Z is the number of considered topics (3). Finally, the average intersensor misalignment ($\overline{\tau}$) is applied to each band of the input slave image to generate the final registered result. It is important to note that we make use of the affine model because this transformation has been shown to be effective for Sentinel Level-1C operational data [12].

III. Experiments

A. Data Sets

Four coupled S2 MSI and S3 OLCI image sets have been used for the experiments (Fig. 2). All the considered images are operational data products downloaded from the Copernicus Open Access Hub (https://goo.gl/uXmPxL). In addition, they have been processed using the Sentinel Application Platform (SNAP) software by resampling the S2 MSI product

to 20-mpp spatial resolution and reprojecting the S3 OLCI image to the corresponding S2 tile. The products have been also atmospherically corrected, generating a final size of $5490 \times 5490 \times 13$ pixels in S2 and $366 \times 366 \times 21$ in S3.

1) *Andujar (AN):* The first image set contains two S2 and S3 data products acquired over the Sierra de Andújar (Spain). In particular, both images were captured on March 10, 2017, and they cover between (38.84°, −4.15°) and (37.85°, −2.88°) latitude/longitude coordinates.
2) *Bourdeaux (BR):* The second set consists of a coupled S2 and S3 images, collected over Bourdeaux (France). Specifically, these products were gathered on March 10, 2017, and they include between (45.14°, −1.72°) and (44.13°, −0.37°) coordinates.
3) *Madrid (MA):* The third collection is made up of two S2 and S3 images captured over Madrid (Spain) on April 9 and 10, 2017, respectively. Both products comprise between the (40.64°, −4.18°) and (39.66°, −2.88°) coordinates.
4) *Utrecht (UT):* The fourth image set includes two aerial shots of Utrecht (The Netherlands) which were both acquired on December 27, 2017. The sensing area covers between (52.34°, 4.46°) and (51.32°, 6.01°) coordinates.

B. Experimental Protocol

Different registration experiments have been conducted to assess the proposed approach performance. For each data set, the S2 product has been used as the master image and the S3 counterpart as the slave one. Moreover, a controlled affine transformation has been applied to each S3 product in order to slightly amplify the original MSI and OLCI operational data misalignments. Since there is a 15× spatial difference between the images, the simulated transformations have been defined not to affect the initial slave image scale (details in https://goo.gl/cwAjVS). Regarding the tested methods, five different embedding procedures have been considered: 1) PCA1-PCA1, which projects both master and slave images to their first PCA components where the affine transformation is estimated; 2) PCA2-PCA2, which carries out the registration over the two first PCA components and computes the average intersensor misalignment; 3) PCA3-PCA3, which follows the same process as 2) but with the three first PCA components; 4) Band-PCA1, which uses the master first PCA component to register each individual slave band; and 5) Band-Band, which conducts a band-to-band registration where each slave band is aligned to the closest master one. All these registration mechanisms make use of the same MI-based registration procedure than the proposed approach. Additionally, the 6) phase correlation method [6] has been selected as an alternative band-to-band registration mechanism. To relieve the intersensor spatial differences, S2 images have been subsampled by a 15× factor. Finally, the root-mean-squared error (RMSE) and MI have been used as quantitative metrics.

C. Results

Table I presents a quantitative assessment for the considered data and methods in terms of the RMSE and MI metrics. Specifically, the four data sets are provided in rows and the columns represent the registration alternatives, i.e., (0) No-Reg, (1) PCA1-PCA1, (2) PCA2-PCA2, (3) PCA3-PCA3, (4) Band-PCA1, (5) Band-Band, (6) Phase-Corr, and (7) Proposed. The last row also shows the average metric results, where the best values are highlighted in bold. In addition, Fig. 2 highlights the registration result of the proposed approach.

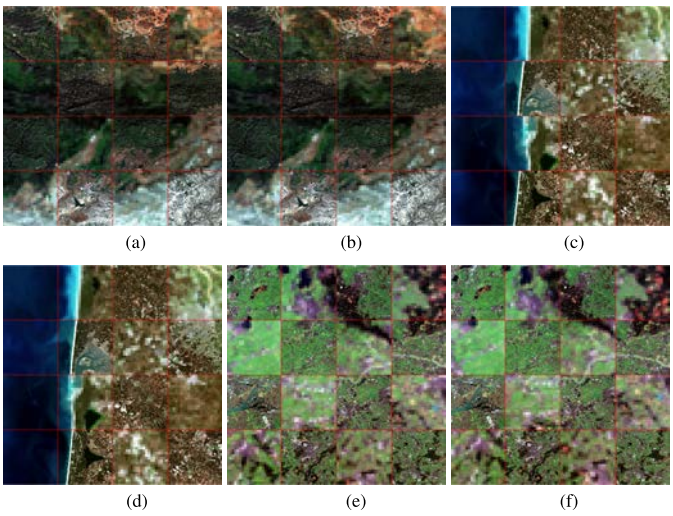

Fig. 2. Qualitative registration results for AN, BR, and UT data sets. (a) AN—NoReg. (b) AN—Proposed. (c) BR—NoReg. (d) BR—Proposed. (e) UT—NoReg. (f) UT—Proposed.

One of the first remarkable points is the advantage of using an intersensor registration scheme within the S2 and S3 contexts. As it was previously mentioned, MSI has a substantially higher spatial resolution than OLCI. Therefore, S2 imagery can be considered a valid ground-truth reference for spatially correcting S3 products. Logically, the higher the sensor spatial resolution, the lower the nominal geolocation errors. In this sense, the quantitative results show that S2 MSI data can be used to effectively register S3 OLCI operational products despite the spatial resolution differences. This fact is also supported by the reported qualitative results (Fig. 2), where the proposed intersensor registration approach is able to correct the existing spatial deviations.

Regarding the overall performance, Table I shows that all the considered intersensor registration alternatives are able to outperform the baseline scenario: (0) No-Reg, where no registration is applied. Considering the RMSE index, the two worst approaches were (3) and (6), followed by (4), (1), (5), and (2). In the case of the MI metric, a similar trend can be observed where (3) and (6) are still the worse methods, followed by (1), (5), (2), and (4). Despite the remarkable performance achieved by some methods, i.e., (2) and (5), the proposed approach is able to provide even a superior result for both metrics. The presented method quantitatively outperforms (2) by 27.95 RMSE and 0.0003 MI units, and it also improves (5) average result in 33.67 RMSE and 0.0004 MI units.

In general, registering intersensor operational data raises the challenge of dealing with different instruments, which is particularly relevant in the Copernicus context due to the significant spatial differences between S2 MSI and S3 OLCI.

TABLE I
QUANTITATIVE REGISTRATION RESULTS FOR THE CONDUCTED EXPERIMENTS

Dataset	(0) No-Reg		(1) PCA1-PCA1		(2) PCA2-PCA2		(3) PCA3-PCA3		(04) Band-PCA1		(5) Band-Band		(6) Phase-Corr		(7) Proposed	
	RMSE	MI	RMSE	MI	RMSE	MI	RMSE	MI	RMSE	MI	RMSE	MI	RMSE	MI	RMSE	MI
AN	11004.21	8.5894	5332.26	8.6430	5306.07	8.6427	5285.51	8.6432	5282.11	8.6433	5280.17	8.6432	8979.10	8.6309	5238.03	8.6425
BR	13369.48	6.5634	5231.95	6.7237	5221.32	6.7251	5323.36	6.7251	5252.37	6.7265	5218.24	6.7250	9484.06	6.6508	5198.43	6.7259
MA	15648.41	8.8218	6460.68	8.8706	6441.18	8.8711	6559.80	8.8706	6496.11	8.8709	6486.58	8.8710	13328.33	8.8535	6448.55	8.8710
UT	16056.75	7.6188	7639.06	7.6201	7617.33	7.6227	23091.32	5.0434	7655.48	7.6214	7623.77	7.6218	11712.95	7.6317	7589.08	7.6232
AVG	14019.71	7.8984	6165.99	7.9644	6146.48	7.9654	10065.00	7.3206	6171.52	7.9655	6152.19	7.9653	10876.11	7.9417	**6118.52**	**7.9657**

Despite its simplicity, the band-to-band registration approach shows a robust performance. However, registering the first two PCA components provides a better overall result, excluding the proposed approach, because the input multispectral domains are encapsulated into the greatest variance directions. In this way, the registration process can be conducted over correlated principal components, which allows unifying the intersensor content. With all these considerations in mind, there is a key factor that makes the proposed approach more suitable to tackle this task: the intersensor noise. Note that MSI and OLCI are affected by different kinds of noise since they both have rather different imaging models and corrections. Therefore, it is possible that different intersensor noises were captured when including more principal components, which logically has a negative impact on the registration process. Precisely, this is the reason why (3) is the worst method, whereas (2) is among the best ones. The proposed approach manages to relieve these undesirable effects by using a multispectral semantic embedding that unifies intersensor data at a higher abstraction level. More specifically, the presented method makes use of the pLSA model to project the S2 MSI and S3 OLCI data into their corresponding generative feature patterns. Hence, the intersensor registration process can be conducted in a common space where visual concepts can be represented via different multispectral signatures while minimizing the effect of raw spectral data noise. Despite the advantages of the proposed intersensor semantic embedding, its performance with other instruments may depend on the considered transformation models and metrics [12]. Further analyses should be made on the EM-based optimization cost for its actual operational deployment.

IV. CONCLUSION

This letter presents an intersensor registration approach to effectively coregister S2 MSI and S3 OLCI operational data. Traditional registration mechanisms struggle at generating a common characterization space when considering MSIs of a different nature. However, the proposed method projects the master and slave input data into a semantic embedding via topic modeling, where the registration process can be conducted at a higher characterization level. The input images are represented according to their spectral feature patterns that represent the same visual concepts across the sensors. Then, a straightforward operational registration procedure is effectively used to estimate the global intersensor displacement over this semantic space. Our experiments, which include four operational data collections and six different registration alternatives, reveal that the presented intersensor registration framework is able to provide advantages in the context of the Copernicus program. This letter proves the potential of probabilistic topic models to effectively uncover intersensor patterns, useful to coregister S2 MSI and S3 OLCI operational data. Future work will be focused on developing efficient parallel implementations of the proposed approach and studying deep intersensor embedding architectures.

REFERENCES

[1] R. Fernandez-Beltran, J. M. Haut, M. E. Paoletti, J. Plaza, A. Plaza, and F. Pla, "Remote sensing image fusion using hierarchical multimodal probabilistic latent semantic analysis," *IEEE J. Sel. Topics Appl. Earth Observ. Remote Sens.*, vol. 11, no. 12, pp. 4982–4993, Dec. 2018.

[2] C. Zhang, G. Li, and W. Cui, "High-resolution remote sensing image change detection by statistical-object-based method," *IEEE J. Sel. Topics Appl. Earth Observ. Remote Sens.*, vol. 11, no. 7, pp. 2440–2447, Jul. 2018.

[3] X. Lu, X. Zheng, and Y. Yuan, "Remote sensing scene classification by unsupervised representation learning," *IEEE Trans. Geosci. Remote Sens.*, vol. 55, no. 9, pp. 5148–5157, Sep. 2017.

[4] R. Fernandez-Beltran, P. Latorre-Carmona, and F. Pla, "Single-frame super-resolution in remote sensing: A practical overview," *Int. J. Remote Sens.*, vol. 38, no. 1, pp. 314–354, 2017.

[5] B. Zitová and J. Flusser, "Image registration methods: A survey," *Image Vis. Comput.*, vol. 21, no. 11, pp. 977–1000, 2003.

[6] J. L. Moigne, N. S. Netanyahu, and R. D. Eastman, *Image Registration for Remote Sensing*. Cambridge, U.K.: Cambridge Univ Press, 2011.

[7] M. Drusch *et al.*, "Sentinel-2: ESA's optical high-resolution mission for GMES operational services," *Remote Sens. Environ.*, vol. 120, pp. 25–36, May 2012.

[8] C. Donlon *et al.*, "The global monitoring for environment and security (GMES) sentinel-3 mission," *Remote Sens. Environ.*, vol. 120, pp. 37–57, May 2012.

[9] W. Ma *et al.*, "Remote sensing image registration with modified sift and enhanced feature matching," *IEEE Geosci. Remote Sens. Lett.*, vol. 14, no. 1, pp. 3–7, Jan. 2017.

[10] J. Fan, Y. Wu, F. Wang, P. Zhang, and M. Li, "New point matching algorithm using sparse representation of image patch feature for SAR image registration," *IEEE Trans. Geosci. Remote Sens.*, vol. 55, no. 3, pp. 1498–1510, Mar. 2017.

[11] Z. Yang, T. Dan, and Y. Yang, "Multi-temporal remote sensing image registration using deep convolutional features," *IEEE Access*, vol. 6, pp. 38544–38555, 2018.

[12] L. Yan, D. P. Roy, H. Zhang, J. Li, and H. Huang, "An automated approach for sub-pixel registration of Landsat-8 operational land imager (OLI) and Sentinel-2 multi spectral instrument (MSI) imagery," *Remote Sens.*, vol. 8, no. 6, p. 520, 2016.

[13] Q. Zhang, Z. Cao, Z. Hu, Y. Jia, and X. Wu, "Joint image registration and fusion for panchromatic and multispectral images," *IEEE Geosci. Remote Sens. Lett.*, vol. 12, no. 3, pp. 467–471, Mar. 2015.

[14] H. Goncalves, L. Corte-Real, and J. A. Goncalves, "Automatic image registration through image segmentation and sift," *IEEE Trans. Geosci. Remote Sens.*, vol. 49, no. 7, pp. 2589–2600, Jul. 2011.

[15] R. Fernandez-Beltran, A. Plaza, J. Plaza, and F. Pla, "Hyperspectral unmixing based on dual-depth sparse probabilistic latent semantic analysis," *IEEE Trans. Geosci. Remote Sens.*, vol. 56, no. 11, pp. 6344–6360, Nov. 2018.

[16] R. Fernandez-Beltran and F. Pla, "Latent topics-based relevance feedback for video retrieval," *Pattern Recognit.*, vol. 51, pp. 72–84, Mar. 2016.

[17] R. Fernandez-Beltran, and F. Pla, "Prior-based probabilistic latent semantic analysis for multimedia retrieval," *Multimedia Tools Appl.*, vol. 77, no. 13, p. 16771–16793, Jul. 2018.

[18] M. Styner, C. Brechbuhler, G. Szckely, and G. Gerig, "Parametric estimate of intensity inhomogeneities applied to MRI," *IEEE Trans. Med. Imag.*, vol. 19, no. 3, pp. 153–165, Mar. 2000.